Journal of Power Sources 271 (2014) 55–59

Contents lists available at ScienceDirect

Journal of Power Sources

journal homepage: www.elsevier.com/locate/jpowsour

Short communication

Hollow spherical $La_{0.8}Sr_{0.2}MnO_3$ perovskite oxide with enhanced catalytic activities for the oxygen reduction reaction

Fanliang Lu [a], Jing Sui [b], Jianmin Su [a], Chao Jin [a, *], Ming Shen [c], Ruizhi Yang [a, *]

[a] College of Physics, Optoelectronics and Energy & Collaborative Innovation Center of Suzhou Nano Science and Technology, Soochow University, Suzhou 215006, China
[b] College of Materials Science and Engineering, Qingdao University of Science and Technology, Qingdao 266042, China
[c] Huasheng Chemical Corporation, Zhangjiagang, Jiangsu 215635, China

HIGHLIGHTS

- A new carbonate-template route to prepared hollow spherical structure was developed.
- Hollow spherical $La_{0.8}Sr_{0.2}MnO_3$ perovskite oxide was prepared.
- HS-LSM has efficient catalytic activity for the ORR.
- The ORR mainly favors a direct four electron pathway.
- HS-LSM exhibits excellent stability for the ORR.

ARTICLE INFO

Article history:
Received 9 July 2014
Accepted 17 July 2014
Available online 1 August 2014

Keywords:
Oxygen reduction reaction
Catalyst
Perovskite oxide
Hollow sphere

ABSTRACT

A hollow spherical $La_{0.8}Sr_{0.2}MnO_3$ (HS-LSM) perovskite oxide has been prepared using a new carbonate-template route, and characterized by XRD, SEM and TEM. SEM and TEM results show that the pre-prepared oxides consist of porous microspheres composed of submicrometer-sized subunits with a secondary particle diameter of ~20–50 nm. The catalytic activity of the oxide for the oxygen reduction reaction (ORR) in 0.1 M KOH solution has been studied using a rotating ring-disk electrode (RRDE). In the ORR tests, a maximum cathodic current density of 6.4 mA cm^{-2} at −0.9 V (vs. Ag/AgCl) with 2500 rpm has been obtained, and the ORR mainly favors a direct four-electron pathway. The chronoamperometric test shows that the HS-LSM exhibits excellent stability for the ORR.

1. Introduction

In recent years, metal–air batteries such as Zn–air (1350 Wh kg^{-1}) and Li–air (11,140 Wh kg^{-1}) have attracted increasing attention due to their high theoretical specific energy density and low environmental impact [1–3]. The low round-trip efficiency and cycle stability of metal–air batteries, however, restrict their applications. Noble metals such as Pt, Au and Au alloys have been extensively investigated as efficient electrocatalysts for gas diffusion-type oxygen reduction and evolution electrodes. Despite the increase in efficiency obtained with such electrocatalysts, the high cost of noble metal limits their large-scale utilization. The development of a novel non-noble metal electrocatalyst with high catalytic activity is an important way to improve the commercial applicability of metal–air batteries.

Among the various types of electrocatalysts, perovskite materials with the formula ABO_3, or $A_{1-x}A'_xB_{1-y}B'_yO_3$ where A or A′ is a rare-earth or alkaline-earth metal (La, Ce, Sr, Ca …) and B or B′ is a transition metal (Fe, Mn, Co…), form an important class. Perovskite electrocatalysts can achieve high catalytic activity and stability for the oxygen reduction reaction (ORR) in metal air batteries because of their defective structures and excellent oxygen mobility. $LaMnO_3$ exhibits high catalytic activity, due to its defective cation-deficient lattice, and the presence of manganese in two oxidation states (Mn^{3+}/Mn^{4+}), resulting in a relatively stable and constant oxygen excess [4]. The catalytic activity of $LaMnO_3$ perovskite can be further enhanced by partial substitution of La or Mn. This induces oxygen vacancies and results in the formation of a larger proportion of metal ions in unstable oxidation states, as well as an overall enhancement of oxygen mobility. $La_{1-x}Sr_xMnO_3$ perovskites, for example, are more active than $LaMnO_3$ in terms of oxygen

* Corresponding authors. Tel.: +86 512 67875503.
E-mail addresses: jinchao@suda.edu.cn (C. Jin), yangrz@suda.edu.cn (R. Yang).

http://dx.doi.org/10.1016/j.jpowsour.2014.07.160
0378-7753/

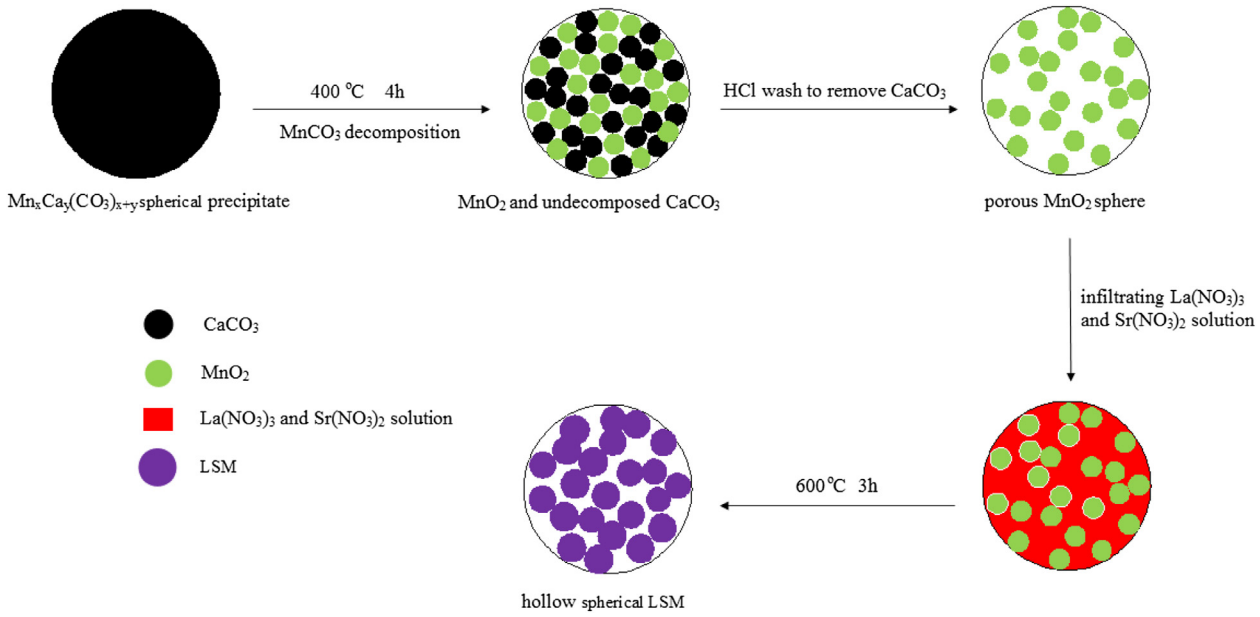

Fig. 1. Schematic diagram of the growing process of the hollow spherical LSM.

reduction in an ambient temperature alkaline 1 M KOH electrolyte [5]. One of the most frequently-used cathode materials in solid oxide fuel cells, $La_{0.8}Sr_{0.2}MnO_3$ (LSM) perovskite oxide has demonstrated promising catalytic properties in a Li–air battery with non-aqueous electrolyte [6,7].

It is well known that ORR is an interfacial reaction, or surface reaction, and the adsorption and dissociation of oxygen molecules mainly occurs in the interface or surface of the catalyst. The more effective reactive sites on the catalyst, therefore, the better the catalytic activity [8]. While $La_{0.8}Sr_{0.2}MnO_3$ perovskite oxides exhibit good electrocatalytic activities, they have little specific surface area, see Yu et al. [7]. In our previous work [9], we have synthesized urchin-like LSM perovskite oxide with a high specific surface area of 48 $m^2\ g^{-1}$, which exhibits better catalytic performances than regular LSM particles. It is necessary and meaningful, therefore, to investigate the structural design of LSM in order to improve its catalytic performance. Among various types of structural designs, hollow spheres are preponderant due to their high surface area, especially with the presence of through-channels on the walls. Such structures provide a larger electrochemical active surface area and improve the mass transfer [10–12].

In this communication, a new carbonate-template route to design and fabricate hollow spheres of $La_{0.8}Sr_{0.2}MnO_3$ perovskite oxide was developed. The catalytical activities of these LSM hollow spheres for the oxygen reduction reaction in an alkaline medium were characterized using rotating-ring-disk electrode (RRDE) testing.

2. Experimental

2.1. Preparation of the spherical carbonate template

In a typical synthesis of the spherical carbonate template, $CaCl_2$ and $Mn(CH_3COO)_2$ were used as starting reagents. $CaCl_2$ and $Mn(CH_3COO)_2$ (20 mmol, in a molar ratio 1:1) were dissolved in 100 ml deionized water, then 5 mmol sodium dodecylsulfate (SDS) was added and stirred constantly, this mixed solution being denoted solution A. Na_2CO_3 (20 mmol) was dissolved in 100 ml deionized water to form solution B. Subsequently solution B was poured into solution A and vigorously stirred to precipitate for 1 h at room temperature. The white precipitates were collected using a centrifuge, and washed with deionized water and ethanol several times to remove impurities. Finally, the spherical $Mn_xCa_y(CO_3)_{2(x+y)}$ templates were dried at 60 °C overnight.

2.2. Preparation of hollow spherical $La_{0.8}Sr_{0.2}MnO_3$

As shown in Fig. 1, the pre-prepared spherical $Mn_xCa_y(CO_3)_{2(x+y)}$ templates were first calcined at 400 °C for 4 h to form MnO_2 spheres, which disperse through the undecomposed $CaCO_3$ spheres. Secondly, the undecomposed $CaCO_3$ spheres were removed by washing with acetic acid (0.2 M) two times, leaving the porous hollow MnO_2 structure. These were washed with distilled water and ethanol several times and dried at 60 °C overnight. Thirdly, 9.6 mmol $La(NO_3)_3{\cdot}6H_2O$ and 2.4 mmol $Sr(NO_3)_2$ were dissolved in 20 ml distilled water to form a mixed solution, which was infiltrated into the pre-prepared porous hollow MnO_2 matrix. This mixture was first dried at 200 °C and then heated to 400 °C, to decompose the nitrites. After several impregnating, drying and firing steps, the dried precursors were finally calcined at 600 °C for 3 h to obtain hollow spherical $La_{0.8}Sr_{0.2}MnO_3$ perovskite oxide (denoted as HS-LSM).

2.3. Characterization of the hollow spherical $La_{0.8}Sr_{0.2}MnO_3$

The crystal structure of the hollow spherical $La_{0.8}Sr_{0.2}MnO_3$ perovskite oxide was examined through X-ray diffraction (XRD) using a Bede D1 X-ray diffractometer (Bede Scientific Ltd., UK; Cu K_α radiation; operated at 40 kV, 45 mA; $\lambda = 0.15418$ nm), the diffraction angle ranging from 20° to 80° with a step of 0.02°and a rate of 1.2° min^{-1}. The oxide morphology was characterized by a scanning electron microscope (SEM, Hitachi SU8010) and a transmission electron microscope (TEM; TecnaiG220 operating at 200 kV).

2.4. Electrochemical measurements

The electrode preparation and electrochemical tests were similar to those presented in our previous works [9,13,14]. The

electrocatalytic activity for the ORR was studied with the RRDE technique using a Pine Electrochemical system (AFMSRX rotator, and AFCBP1 bipotentiostat). The RRDE electrode consisted of a catalyst film-coated GC disk (with a geometric surface area of 0.196 cm^2) surrounded by a Pt ring (with a geometric surface area of 0.125 cm^2). A conventional three-electrode single-compartment Pyrex glass cell was used to carry out the electrochemical investigations at room temperature. A Pt-wire was used as the counter electrode (with a geometric surface area of 0.316 cm^2immersed in the electrolyte solution), and an Ag/AgCl (1 M Cl^-, 0.197 V vs. SHE) reference electrode was used in a double-junction reference chamber. All potential values mentioned in the text are given against this reference only. The electrolyte was 0.1 M KOH solution prepared with ultrapure water (Millipore, 18.2 MΩ cm).

The catalyst ink of the HS-LSM was made by mixing 5 mg of HS-LSM powder and 5 mg of acetylene black with 95 μl of Nafion solution (5–6 wt.% in ethanol) and 350 μl of ethanol in an ultrasonic bath for 2 h. The working electrode was prepared by applying 7 μl of catalyst ink onto the surface of the GC electrode with a micropipette and drying in air for 0.5 h. The catalyst loading was 0.4013 mg cm^{-2}. For comparison, samples of commercial $La_{0.8}Sr_{0.2}MnO_3$ (bought from fuel cell materials, denoted as C-LSM), and urchin-like $La_{0.8}Sr_{0.2}MnO_3$ (denoted as U-LSM), were prepared and tested with the same procedure.

RRDE voltammetric experiments were performed for ORR test with a 10 mV s^{-1} scanning rate in an O_2-saturated 0.1 M KOH solution, at room temperature. The voltage scanning range was from −1.0 to 0.2 V. The ring potential was set at 0.5 V, which is considered to be sufficiently high to induce complete peroxide decomposition [15]. During the ORR test, the background capacitive current contribution (obtained from an N_2-saturated experiment) is subtracted from each voltammogram. Prior to each measurement, the KOH solution was bubbled with either N_2 or O_2 at a flow rate of 100 standard cubic centimeters per minute (sccm) over 0.5 h.

3. Results and discussion

3.1. Structure and morphology characterization

Fig. 2 presents X-ray diffraction (XRD) patterns of hollow spherical LSM powders after they were calcined at 600 °C for 3 h. Compared with the standard PDF card (PDF # 40-1100), all the characteristic peaks can be well indexed as a perovskite phase with a rhombohedral structure, except that some trace small peaks around 25, 29, 36, 45° correspond to $La(OH)_3$ and/or La_2O_3. No other peaks can be observed, indicating high phase purity of the synthesized sample.

SEM and TEM were used for observing the morphology and microstructure of the products. Fig. 3(a) shows the typical morphologies of MnO_2 intermediates after removing the $CaCO_3$ templates. The image reveals that the MnO_2 intermediates are

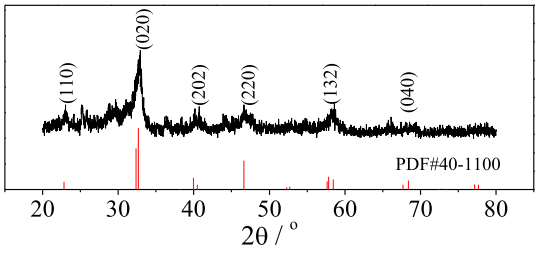

Fig. 2. XRD patterns of the hollow spherical LSM powder calcined at 600 °C for 3 h.

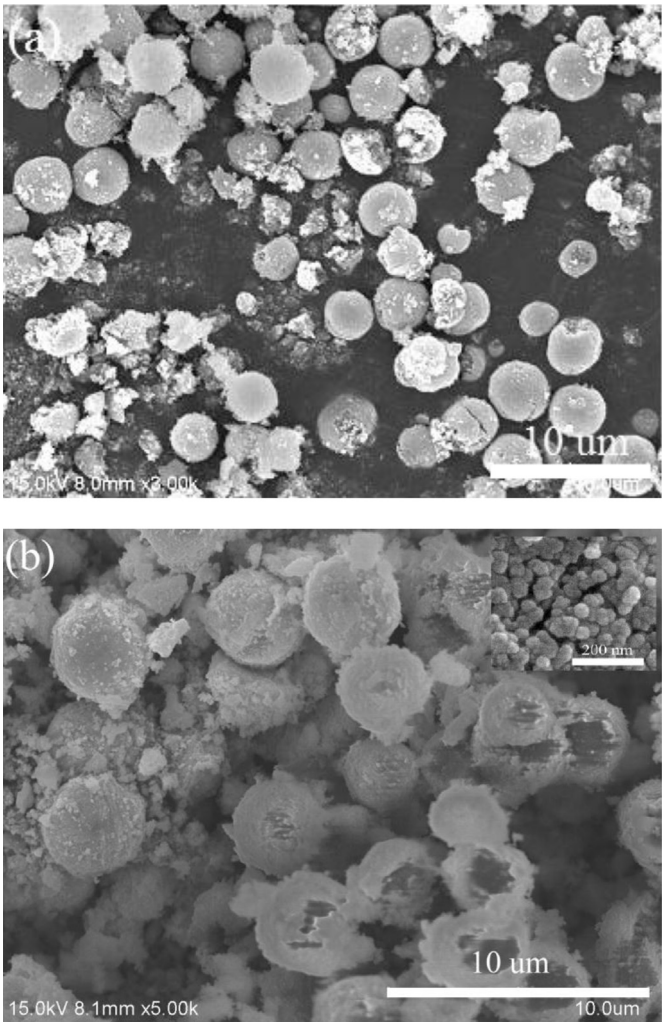

Fig. 3. SEM image of MnO_2 intermediates after washing $CaCO_3$ templates (a); SEM image of the hollow spherical LSM powders calcined at 600 °C for 3 h (b).

composed of hollow porous microspheres with diameters of ~1–3 μm. It is interesting to find that some microspheres have cracks on their surface, indicating that the MnO_2 intermediates have hollow structures. Fig. 3(b) presents the SEM image of the HS-LSM sample. It can be seen clearly that the products are microspheres with diameters of ~1–3 μm, and a great fraction of the microspheres have cracks on their surfaces, suggesting that they have a hollow structure. From the magnified micrograph of one microsphere, in the top right inset in Fig. 3(b), it can be observed that the HS-LSM are porous and composed of submicrometer-sized subunits with a secondary particle diameter of ~20–50 nm. This unique microstructure benefits gas diffusion and can provide more electrochemical reaction sites.

3.2. Electrochemical performance measurements

The electrochemical properties of the HS-LSM were characterized with the RRDE technique. For comparison, commercial $La_{0.8}Sr_{0.2}MnO_3$ (C-LSM), urchin-like $La_{0.8}Sr_{0.2}MnO_3$ (U-LSM) and commercial Pt/C (20 wt.% Pt) were also tested under the same conditions. The measurements were carried out in a cathodic sweep with 10 mV s^{-1} at various rotation speeds (ω) from 400 to 2500 rpm. A comparison of the disk currents obtained from the ORR activities on C-LSMO, U-LSMO, HS-LSM and Pt/C, as measured

with the RRDE at 2500 rpm, is shown in Fig. 4. The onset potential, half-wave potential and diffusion limiting current density of these four catalysts are displayed in Table 1. The ORR activity was found to increase as follows: C-LSM < U-LSM < HS-LSM < Pt/C, as evidenced by the three parameters shown in Table 1. The diffusion limiting current density of HS-LSM reaches that of Pt/C, and a negative shift of about 169 mV exists in the half-wave potential of HS-LSM as compared to Pt/C. It should be noted that the diffusion limiting current density and half-wave potential of the Pt/C are in good agreement with the values of Pt/C (20 wt.% Pt) reported elsewhere [16]. Higher diffusion limiting current density clearly indicates that HS-LSM is more active than C-LSM and U-LSM and is comparable to the activity of Pt/C.

HS-LSM catalyst was further studied using the RRDE technique for the evaluation of the oxygen reduction kinetic parameters. The measurements were carried out in a cathodic sweep with 10 mV s^{-1} at 400, 900, 1600 and 2500 rpm. Fig. 5 shows both ring current density (i_r) and disk current density (i_d) of the HS-LSM catalyst recorded in an O_2-saturated 0.1 M KOH solution, at different rotation speeds. From i_d curves, it can be seen that the diffusion limiting current densities increase as rotation speed increases from 400 to 2500 rpm. Higher rotation speeds lead to faster oxygen flux to the electrode surface, and consequently larger currents. The transferred electron number and the formation of peroxide species (OH_2^-) involved in the ORR are two important parameters to verify the ORR catalytic pathway. The RRDE experiment involves holding the disk at a potential E_d, where the reaction $O + ne \rightarrow R$ produces a cathodic current i_d. The ring is kept at a sufficiently positive potential E_r (0.5 V) such that any R reaching the ring is rapidly oxidized, and the concentration of R at the ring surface is essentially zero [17]. The ring current, i_r, is related to the disk current, i_d, by a quantity N, the capture coefficient. The electron number (n) transferred and the contents of peroxide HO_2^- during the ORR can be calculated, according to the following Equations (1) and (2) [18,19],

$$n = 4\frac{i_d}{i_d + (i_r/N)}, \quad (1)$$

$$HO_2^-\% = 100 \times \frac{2i_r/N}{i_d + (i_r/N)}, \quad (2)$$

where n is the transferred electron number during the ORR process, i_d is the disk current, i_r is the ring current and N is the capture coefficient (here $N = 0.22$).

The electron number transferred and the quantity of peroxide HO_2^- generated during the ORR at 400, 900, 4600 and 2500 rpm are calculated and displayed in Fig. 6. The n values are 3.8–4.0 over the potential range from −0.9 to 0 V (vs Ag/AgCl), suggesting that the HS-LSM catalyst most likely favors the $4e^-$ reduction reaction process. The measured % HO_2^- yield is below 8.0% over the potential range of −0.9 to 0 V, giving an electron transfer number of 3.8–4.0.

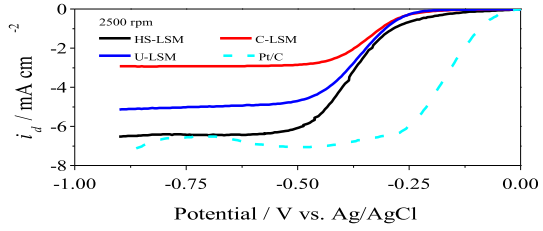

Fig. 4. Comparisons of electrochemical catalytic activities for the ORR among the commercial LSM (C-LSM), the urchin-like LSM (LSM), the hollow spherical LSM (HS-LSM) and commercial Pt/C electrocatalysts at the same conditions.

Table 1
Summary of the ORR catalytic characteristics of C-LSM, U-LSM, HS-LSM and Pt/C.

Catalyst	Onset potential (V vs. Ag/AgCl)	Half-wave potential (V vs. Ag/AgCl)	Current density (mA cm^{-2})
C-LSM	−0.211	−0.374	−4.94
U-LSM	−0.196	−0.367	−5.14
HS-LSM	−0.149	−0.338	−6.46
Pt/C	0.003	−0.169	−7.14

The stabilities of HS-LSM and commercial Pt/C catalysts for the ORR were examined with the chronoamperometric method in an O_2-saturated 0.1 M KOH at 2500 rpm. The ORR potential was selected to be −0.3 V vs. Ag/AgCl, and the results obtained are shown in Fig. 7. It can be seen that a rapid 22% loss of the current density occurs for the commercial Pt/C catalyst in the initial 5000 s of operation, before remaining stable over the testing period. Impressively, the ORR current density of HS-LSM presents a slow downtrend, only decreasing by 9.5% after 60,000 s of continuous operation. There are many potential causes of this attenuation, such

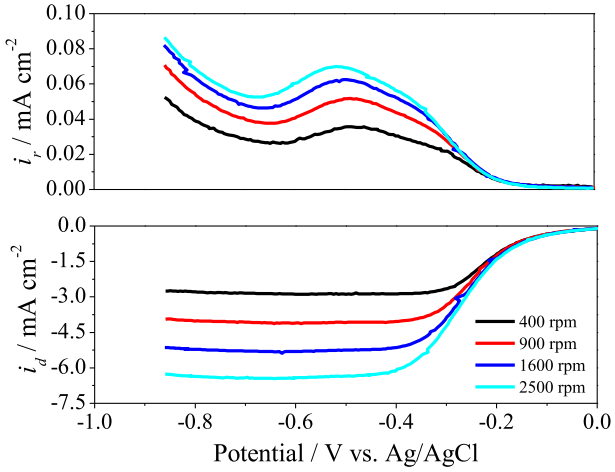

Fig. 5. Disk current density (i_d) and ring current density (i_r) collected on the HS-LSM/C electrode during the ORR in O_2 saturated 0.1 M KOH solution.

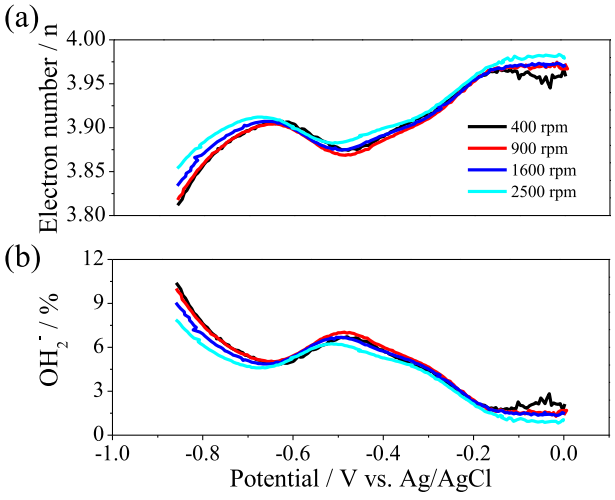

Fig. 6. Electron transfer number (n) and peroxide HO_2^- calculated with i_d and i_r at various rotation speeds.

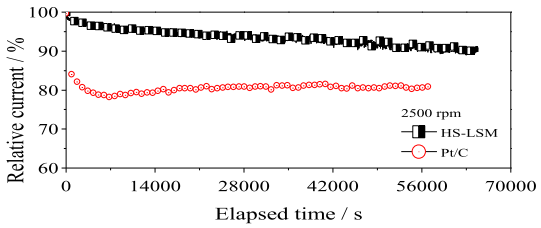

Fig. 7. Current–time (i–t) chronoamperometric responses for the ORR at the HS-LSM and the commercial Pt/C catalyst in an O_2 saturated 0.1 M KOH solution at −0.30 V (vs. Ag/AgCl) at 2500 rpm.

as changes in the microstructure of the electrode, aggregation of the electrocatalyst or change of the electrolyte concentration [20]. The stability of the electrocatalyst is clearly a critical issue, but it is not the main topic of this work.

4. Conclusions

In summary, hollow spherical $La_{0.8}Sr_{0.2}MnO_3$ (HS-LSM) perovskite oxides were prepared using a new carbonate-template route. The HS-LSM has shown high activity for the ORR in alkaline solution and a four-electron pathway is dominant for the ORR. The HS-LSM is found to be quite stable for the ORR, outperforming the commercial Pt/C. The results show that HS-LSM could be used as a promising electrocatalyst candidate for the ORR in fuel cells and metal–air batteries.

Acknowledgments

The project was supported by National Natural Science Foundation of China (51272167, 21206101), Natural Science Foundation of Jiangsu Province, China (BK20141199), Natural Science Foundation of the Higher Education Institutions of Jiangsu Province, China (14KJB480005), Specialized Research Fund for the Doctoral Program of Higher Education (20133201120005), and the ministry of education to study abroad returned funds.

References

[1] M. Armand, J.M. Tarascon, Nature 451 (2008) 652–657.
[2] G. Girishkumar, B. McCloskey, A.C. Luntz, S. Swanson, W. Wilcke, J. Phys. Chem. Lett. 1 (2010) 2193–2203.
[3] F.Y. Cheng, J. Chen, Chem. Soc. Rev. 41 (2012) 2172–2192.
[4] J. Suntivich, H.A. Gasteiger, N. Yabuuchi, H. Nakanishi, J.B. Goodenough, Y. Shao-Horn, Nat. Chem. 3 (2011) 546–550.
[5] J. Tulloch, S.W. Donne, J. Power Sources 188 (2009) 359–364.
[6] A. Débart, J. Bao, G. Armstrong, P.G. Bruce, J. Power Sources 174 (2007) 1177–1182.
[7] Z.H. Fu, X.J. Lin, T. Huang, A.H. Yu, J. Solid State Electrochem. 16 (2012) 1447–1452.
[8] Y.J. Wang, D.P. Wilkinson, J. Zhang, Chem. Rev. 111 (2011) 7625–7651.
[9] C. Jin, X.C. Cao, L.Y. Zhang, C. Zhang, R.Z. Yang, J. Power Sources 241 (2013) 225–230.
[10] Y.L. Yao, Y. Ding, L.S. Ye, X.H. Xia, Carbon 44 (2006) 61–66.
[11] Y. Ding, X.H. Xia, J. Nanosci. Nanotechnol. 6 (2006) 1101–1106.
[12] Y. J Xiong, Y. Xie, Z.Q. Li, C.Z. Wu, R. Zhang, Chem. Commun. 8 (2003) 904–905.
[13] C. Jin, F.L. Lu, X.C. Cao, Z.R. Yang, R.Z. Yang, J. Mater. Chem. A 1 (2013) 12170–12177.
[14] C. Jin, X.C. Cao, F.L. Lu, Z.R. Yang, R.Z. Yang, ACS Appl. Mater. Interfaces 6 (2014) 847–853.
[15] J. Sunarso, A.A. Torriero, W. Zhou, P.C. Howlett, M. Forsyth, J. Phys. Chem. C 116 (2012) 5827–5834.
[16] J. Wu, Z.R. Yang, X.W. Li, Q.J. Sun, C. Jin, P. Strasser, R.Z. Yang, J. Mater. Chem. A 1 (2013) 9889–9896.
[17] I. Roche, E. Chainet, M. Chatenet, J. Vondrak, J. Phys. Chem. C 111 (2007) 1434–1440.
[18] X.L. Wu, L.Y. Jiang, Y.G. Guo, L.J. Wan, Adv. Mater. 21 (2009) 2710–2714.
[19] T. Hyodo, M. Kayashi, N. Miura, N. Yamazoe, J. Electrochem. Soc. 143 (1996) L266–L271.
[20] F.Y. Cheng, Y. Su, J. Liang, Z.L. Tao, J. Chen, Chem. Mater. 22 (2010) 898–905.